OXFORD

Cerebral Cortex, 2017; 1–14

doi: 10.1093/cercor/bhx133
Original Article

ORIGINAL ARTICLE

Temporally Segmented Directionality in the Motor Cortex

S. B. Suway[1,2], J. Orellana[2], A. J. C. McMorland[3,4], G. W. Fraser[2,5], Z. Liu[6], M. Velliste[3,5,7], S. M. Chase[2,8], R. E. Kass[2,6,9] and A. B. Schwartz[1,2,3,10,11]

[1]Center for Neuroscience, University of Pittsburgh, Pittsburgh, PA 15260, USA, [2]Center for the Neural Basis of Cognition, Carnegie Mellon University and University of Pittsburgh, Pittsburgh, PA 15213, USA, [3]Department of Neurobiology, University of Pittsburgh, Pittsburgh, PA 15260, USA, [4]Centre for Brain Research, University of Auckland, Auckland 1142, New Zealand, [5]Fivetran, San Francisco, CA 94102, USA, [6]Department of Statistics, Carnegie Mellon University, Pittsburgh, PA 15213, USA, [7]Systems Neuroscience Institute, University of Pittsburgh, Pittsburgh, PA 15260, USA, [8]Department of Biomedical Engineering, Carnegie Mellon University, Pittsburgh, PA 15213, USA, [9]Machine Learning Department, Carnegie Mellon University, Pittsburgh, PA 15213, USA, [10]Department of Bioengineering, University of Pittsburgh, Pittsburgh, PA 15260, USA and [11]University of Pittsburgh Brain Institute, University of Pittsburgh, Pittsburgh, PA 15260, USA

S. B. S. and J. O. contributed equally to this work
Address correspondence to A. B. Schwartz, E1440 BST 3500 Terrace St., Pittsburgh, PA 15261, USA. Email: abs21@pitt.edu

Abstract

Developing models of the dynamic and complex patterns of information processing that take place during behavior is a major thrust of systems neuroscience. An underlying assumption of many models is that the same set of rules applies across different conditions. This has been the case for directional tuning during volitional movement; a single cosine function has been remarkably robust for describing the encoding of movement direction in different types of neurons, in many locations of the nervous system, and even across species. However, detailed examination of the tuning time course in motor cortex suggests that direction coding may be labile. Here, we show that there are discrete time epochs within single reaches, between which individual neurons change their tuning. Our findings suggest that motor cortical activity patterns may reflect consistent changes in the state of the control system during center-out reaching. These transitions are likely linked to different behavioral components, suggesting that the task defines changes in the operational structure of the control system.

Key words: cosine tuning, macaque motor cortex, population decoding, segmented processing

Introduction

Understanding and modeling the dynamic activation of neural ensembles is a major goal of systems neurophysiology. The pioneering experiments of Georgopoulos et al. (1982) in which monkeys reached to radial targets from a central start position showed that the tuning relation between single-unit neural firing rates in the motor cortex and movement direction could be fit with a broad cosine tuning function that spanned all movement directions. Direction was shown to be "encoded" in a way that was determined by a neuron's "preferred direction" (PD; direction of peak firing). These features were used in the population vector algorithm (PVA) to extract movement direction from neural activity (Georgopoulos et al. 1983). Cosine tuning has since been shown to be robust for many paradigms and characterizes unit activity recorded in structures throughout the neural axis during movement (Schwartz 1994a, 1994b; van Hemmen and

Schwartz 2008). This type of broad tuning has been expanded to multiple parameters describing the motion of the arm, wrist, and fingers, and, as a general descriptor of upper limb dynamics, forms the basis for brain–computer interfaces in which recorded neural activity drives the movement of external devices (Wessberg et al. 2000; Serruya et al. 2002; Taylor et al. 2002; Hochberg et al. 2006; Wodlinger et al. 2015). However, evidence is accumulating that a cell's PD may be unstable (Sergio and Kalaska 1998; Churchland and Shenoy 2007; Hatsopoulos et al. 2007; Suminski et al. 2015). Directional tuning may even change within the course of a single reaching movement. Because of these rapid changes in a neuron's directional sensitivity, the canonical aspect of a cell's PD and the meaning of directional tuning have been called into question.

We carefully examined changes of direction representation in motor cortical discharge as reaching takes place. In simulation, we determined that complex firing rate patterns and apparent tuning lability can result from neuronal tuning to multiple kinematic variables. However, even though adding more kinematic parameters in the simulation could lead to tuning lability, it did not account for the within-trial changes observed in the actual data. Instead, we found discrete, consistent changes between 3 well-defined epochs across the population of neurons. As we will show, many neurons display stable PDs within each of these epochs. During the sharp transitions between tuning epochs, modulation dropped to a minimum. These transitions corresponded to different phases of the reach, suggesting that the tuning changes were driven by the behavioral structure of the task.

The tuning functions generated in the original center-out experiments compared the "mean" discharge rate, a single number calculated across the duration of movement, to a single movement direction from the center position to the target. When expanding these findings to account for task dynamics, the simplest assumption would be that the model was stationary—the same model would be valid at each time point through the trial. If the hand moves in a straight line from the center position to the radial target, direction-induced neural modulation should be constant during the trial. According to the cosine tuning model, if direction is the only factor governing the firing rate of a neuron, a profile of firing rate versus time, throughout a movement, should be flat (Fig. 1A).

The problem can be formalized with a simple planar model used in the original 2D center-out task:

$$\lambda = \beta_0 + \beta_x D_x + \beta_y D_y, \quad (1)$$

where λ is the firing rate of a cell, D_x, D_y are coordinates of a unit vector pointing in the movement direction, β_0 is baseline firing rate, β_x and β_y are the coordinates of a vector in the cell's PD with modulation depth $m = \sqrt{\beta_x^2 + \beta_y^2}$. If D_x and D_y are constant (straight movement), then the neuron's firing rate should remain unchanged throughout the trial.

Although the basic finding of cosine tuning has been confirmed repeatedly, motor cortical firing during reaching movements is rarely constant. This suggests that either a neuron's discharge rate is governed by additional, non-directional factors (requiring an extension of the original cosine-tuning model) or that the directional specificity of each neuron changes during the reach (with the possibility that direction coding in general may be invalid). Trial-averaged firing rate profiles of motor cortical firing rates are almost always phasic, with peaks and valleys at different points within the reach, resembling the examples shown in Figure 1B or C. This shows that simple direction encoding by these neurons is not, by itself, an adequate description of motor cortical function, motivating investigators to consider the effect of movement variables other than direction on firing rate. The simplest of these are position and its successive derivatives, velocity and acceleration (Ashe and Georgopoulos 1994). In single neurons, interactions between direction and these additional parameters can produce complex changes in firing rate with temporal instability in both the amplitudes and PDs of directional tuning. In this paper, we first confirm the temporal instability of directional tuning during single reaches (Fig. 3), then show that extending the model with non-directional parameters does not account for this observation (see Supplementary Fig. 3). Finally, we describe distinct phases of the reach, defined by each neuron's directional modulation, in which tuning is robust and stable (Figs 4 and 5). This indicates that direction is a major determinant of firing rate, but suggests the existence of distinct states within a single reach. The step-changes in PD, clearly evident in our results (Fig. 4E), signify discrete segmentation of neural processing during reaching.

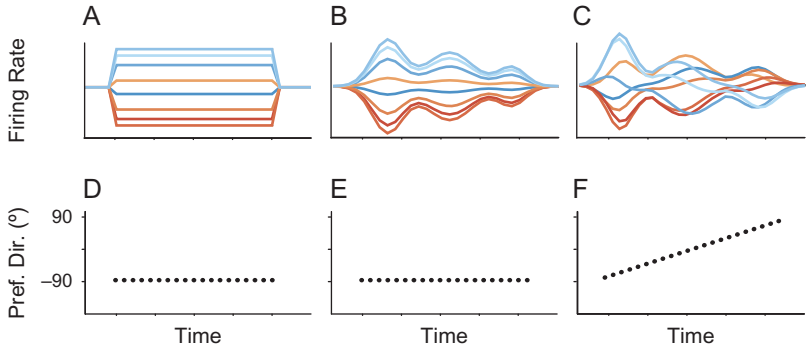

Figure 1. Simulated examples of tuning vs. time. Each example is composed of 8 straight, center-out, point-to-point reaches. The top row is the firing rate time course of the simulated neuron, with colored traces corresponding to movement in a particular direction. The bottom row shows the PD calculated in separate bins throughout the trial. (A,D) A canonical neuron that behaves according to the classic cosine model, in which direction is the only determinant of firing rate. Assuming a straight movement, the firing rate would be a step-function and constant during the movement. The PDs of tuning functions calculated in small windows throughout the trial are constant across windows. (B,E) A more typical firing rate pattern in which the neuron shows several peaks of firing during reaching. In this case, the entire length of the profile is scaled uniformly by direction and the PD is stationary. (C,F) A neuron with varying modulation patterns during the trial. Neural modulation again has multiple components during the reach, but firing rate is both direction- and time- dependent. At each point in time, direction has a different effect on firing rate. In this case, the PD changes continually through the trial.

Materials and Methods

Behavioral Task, Neural Recording, and Neural Data Processing

Rhesus monkeys (*Macaca mulatta*, male, 3 animals) were seated in a primate chair, with one arm restrained. An infrared marker was attached to the free hand and 3D position was monitored at 60 Hz using an Optotrak 3020 motion capture device (Northern Digital Inc.). The monkeys could not see their moving arm, but instead observed a computer monitor showing a virtual reality (VR) environment where the position of the hand was represented by a spherical cursor. The scene was displayed in 3 dimensions using a depth-displaying monitor (Virtual Window, Dimension Technologies Inc.). The monkeys were trained to perform a center-out reaching task in which they had to move the cursor from a starting location toward radial targets equidistant from the center. Workspace radii were 7.4, 6.5, and 8.0 cm for monkeys C, F, and N, respectively. Monkeys C and N performed a version of the task with targets arranged in a 2D plane, while monkey F performed the task with a 3D arrangement of targets (Fig. 2). Monkeys C and F were required to hold the position of the target for a few hundred milliseconds. Monkey N was not required to hold, but instead was allowed to return back to the home position immediately. All movement conditions were presented in a pseudo-random fashion: failed trials were returned to the queue until each set was completed. Monkey C performed 47 repetitions to each of 16 targets; monkey F performed 26 repetitions to each of 26 targets; monkey N performed 40 repetitions to each of 58 targets. Additional information about the data sets is detailed in Supplemental Experimental Procedures 1.

We determined 5 task-related and kinematic events for each trial: Target show, movement onset, peak velocity, movement offset, and the end of a hold period ("hold off"). Movement onset and offset times were defined as the point when hand speed passed 15% of its maximum. Electrical activity from single neurons was recorded extracellularly using chronically implanted 96-channel "Utah" electrode arrays (Blackrock Microsystems) implanted approximately in the arm area of the pre-central gyrus (for locations see Supplementary Fig. 1).

We recorded 93, 119, and 185 single units for C, F, and N, respectively. For monkeys F and N, waveform snippets were stored for each threshold crossing and neuronal spikes were sorted offline using "Offline Sorter" (Plexon Inc.). For monkey C, single units were sorted manually online, with sorts adjusted periodically to maintain isolation as needed. Neural data recorded from monkeys N and C were collected over one day. For monkey F, neural data were collected over 5 consecutive recording days. To average across days, units were identified as being the same using multi-day unit identity analysis (Fraser and Schwartz 2012). This was accomplished by calculating a similarity score derived from 4 independent metrics: Mean firing rate, spike waveform, auto-correlation, and cross-correlation with the rest of the population (see also Supplemental Experimental Procedures 2).

Spike trains from each unit were binned in 20 ms intervals to compute instantaneous firing rate. A Gaussian kernel with standard deviation of 50 ms was used for smoothing. The hand position values were resampled and interpolated to match the time steps of the firing rates using the function "pchip" in Matlab. On each trial, we took movement onset to be time zero and then aligned across trials to additional landmarks at target show, peak velocity, movement offset, and, for monkeys C and F, hold off. This was accomplished by choosing the number of bins between each landmark so that the average bin size was

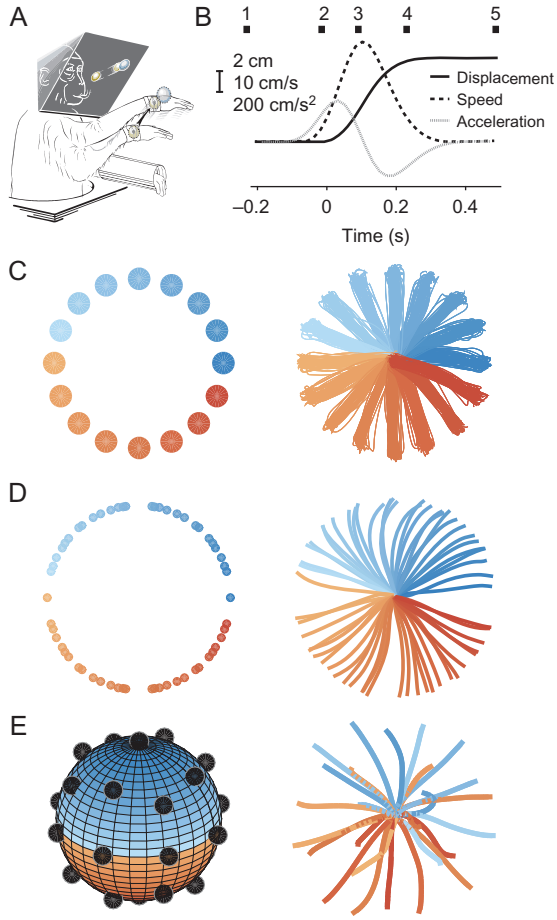

Figure 2. Experimental design and kinematic results. (*A*) Monkeys reached for radial targets displayed in a 3D computer monitor. (*B*) Representative kinematics from a single monkey C experiment. 1 Target display; 2 Movement onset; 3 Peak velocity; 4 End of movement; 5 Reward administration. (*C*) Two-dimensional target arrangement, monkey C. Left—targets individually displayed in VR. Right—Trajectories of the hand collected during one experiment, with all repeated movements shown (47 per target). (*D*) Two-dimensional target arrangement, monkey N. (*E*) Three-dimensional target arrangement, monkey F. Trial-averaged hand trajectories are shown for monkeys N and F. In panels (*C–E*), the color of the targets corresponds to that of the trajectories. See also Supplementary Figure 1 for electrode array placement.

20 ms, and counting the spikes within each bin. Thus, although a single bin spans 20 ms on average, it may span more or less time on a given trial. Because time was normalized independently between each alignment point, each segment of the task was associated with different trial-to-trial variation in bin length. The standard deviation of the bin length during the most variable epoch across our data sets was 6 ms.

Lastly, we normalized firing rate by scaling its value between zero and one based on minimum and maximum firing rate, and subtracting the mean over targets (cross-condition mean) at each time step. Amplitude normalization is critical only for the population vector analyses (described below), but it is also convenient when comparing tuning characteristics between neurons with a different range of firing rates. Subtracting the cross-condition mean allowed us to focus on the dynamics of tuning, rather than dynamics shared across targets. All analyses described below used the time-normalized data. All analyses except those described in Supplementary Figure 3 used the mean-subtracted,

amplitude-normalized changes in firing rates. Analyses described for that figure relate firing rates to kinematic variables, which in principle may modulate spiking irrespective of target (e.g., scalar speed or displacement). These preprocessing steps were, therefore, not performed on data used in those analyses.

We sometimes observed that neurons would fire at rates that were unexpected, based on their typical trial-to-trial variability. If this happened in the same trial for many of the units in the recorded sample, all data for that trial were removed to improve the robustness of nonlinear model fitting (described below). The firing rate profiles from individual units were analyzed as vectors in time. Each trial vector was correlated with all the other trials to that target (using dot products) and if the mean correlation between that trial and all others was below 0.2, it was deemed to be of "high variance." This was repeated for each individual unit in that trial. If more than 84% (the percentile corresponding to mean+1 std on a normal distribution) of the neurons had high variance for that trial, the trial was excluded (for all neurons) from further analysis. Fewer than 15% of trials were excluded due to this criterion. Interestingly, the low firing rate correlation between a given trial and the mean firing rate was not strongly related to kinematic variability, suggesting that the high variability was due to noise, for example from movement artifacts in the neural recordings. Results of individual analyses did not depend critically on this exclusion, though the robustness of nonlinear model fitting ("component fitting," see below) was improved.

PD Stability Test

Tuning functions were calculated using the firing rates in 20 ms increments to determine statistical changes in directional tuning for each unit. We estimated cosine tuning functions from the recorded neural data using least squares linear regression based on the following model:

$$y_i = \beta_0 + \beta_1 \cos(\theta_{targ} - \theta_{PD}) + \varepsilon_i, \quad (2)$$

where $y_i = \hat{\lambda}_i$ is the single-trial estimate of a neuron's firing rate, β_0 is baseline rate, $\theta_{targ} - \theta_{PD}$ is the angle between the target direction and the neuron's PD, and ε_i is the noise (or error) representing the deviation from cosine tuning. We define $\hat{m} = \beta_1$ as the estimated magnitude or modulation depth of the tuning function. The extension to the 3D target arrangement involves expressing the $\cos(\theta_{targ} - \theta_{PD})$ covariate as the dot product of 2 unit-length 3D vectors. Two versions of this model were constructed assuming either that PDs are fixed in time (Eq. 3) or that PDs change over time (Eq. 4). We reasoned that if PDs were actually constant, allowing the fitted PD to vary with time would not significantly improve the likelihood of the model. Furthermore, the variation in firing rate between time bins would be sufficiently described by a change in the modulation depth of the stable tuning function. We thus formulated a "restricted" model with a static PD such that

$$y_{i,t} = \beta_{0,t} + \beta_{1,t} \cos(\theta_{targ} - \theta_{PD}) + \varepsilon_{i,t}, \quad (3)$$

where t denotes time. We then formulated an "unrestricted" model with time-varying PD such that

$$y_{i,t} = \beta_{0,t} + \beta_{1,t} \cos(\theta_{targ} - \theta_{PD_t}) + \varepsilon_{i,t} \quad (4)$$

After fitting, we then summed the log-likelihoods of the model fits at each time bin. To compare the models' relative goodness-of-fit, we performed a likelihood-ratio test. The test statistic is given as

$$D = -2\ln(\text{likelihood of restricted model}) + 2\ln(\text{likelihood of unrestricted model}) \quad (5)$$

The null hypothesis of the test represents the case that the restricted (i.e., constant PD) model is as likely as the unrestricted (i.e., time-variant PD) model, given the data. The value of D under the null hypothesis is assumed to follow a chi-squared distribution with degrees of freedom equal to the difference in degrees of freedom between the 2 models. The restricted model had 1 + T degrees of freedom in the 2D target case, or 2 + T in the 3D case: one (or two) from θ_{PD}, and T from the $\beta_{1,t}$ parameters, where T is the number of time steps in the testing period. The unrestricted model had 2T degrees of freedom in the 2D target case, or 3T in the 3D case: T (or 2T) from θ_{PD_t} and T from the $\beta_{1,t}$ parameters. For the likelihood ratio test, this gives T – 1 dfs for the 2D target case, or 2T – 2 dfs for the 3D target case. We failed to reject the null hypothesis of "PD stability" if the P-value of this test exceeded (0.05/number of time bins considered). To reduce the influence of noise, time bins for which a neuron was not significantly modulated by target direction (one-way ANOVA, $P > 0.001$) were excluded from the analysis. This is important because it allows us to be sure that a result of "stable PD" cannot be attributed to a lack of tuning; a model with changing PD does not improve likelihood over a model with static PD if there is no task-related modulation of firing.

We note that θ_{targ} in Equations (2)–(4) represents the target direction (constant throughout a trial), rather than the instantaneous direction of the hand end-point. This is in contrast to the methods utilized in Supplementary Figures 2 and 3, which used the instantaneous hand direction. We found there was consistent modulation of many units after the hand had stopped, which is not expected for a model based solely on instantaneous hand direction (see, for example, Supplementary Fig. 2*B*, left subpanel). Using the true hand direction was therefore only valid for part of the trial. Instead, cosine tuning to target direction was consistently found to be robust at most time points in the trial (Fig. 3*B*).

Tuning Reliability Over Time

Trial-to-trial reliability of PD estimates (Eq. 2) at each 20 ms time bin was assessed by bootstrap. We first found the PD within each time bin for each unit using the original sample of data. Firing rates for each unit were then sampled with replacement across trials 1000 times. At each time bin, a distribution of unsigned angles was formed by finding the arccosine of the dot product between the unit vectors representing the original PD estimate and each of the bootstrap estimates of PD (from the trial resampling). We then found the 95% confidence interval of these angles from the percentiles of this distribution. This interval is described for the population of neurons in Figure 3*A*.

Component Fitting

Our 20 ms tuning analysis showed that PDs tended to change in discrete steps during the reach. These steps, or segments, had durations of 100–150 ms and we used a novel component-fitting procedure to identify each tuning epoch (Eq. 6). Inspection of the sequential tuning functions along with firing rate profiles revealed that the modulation depths

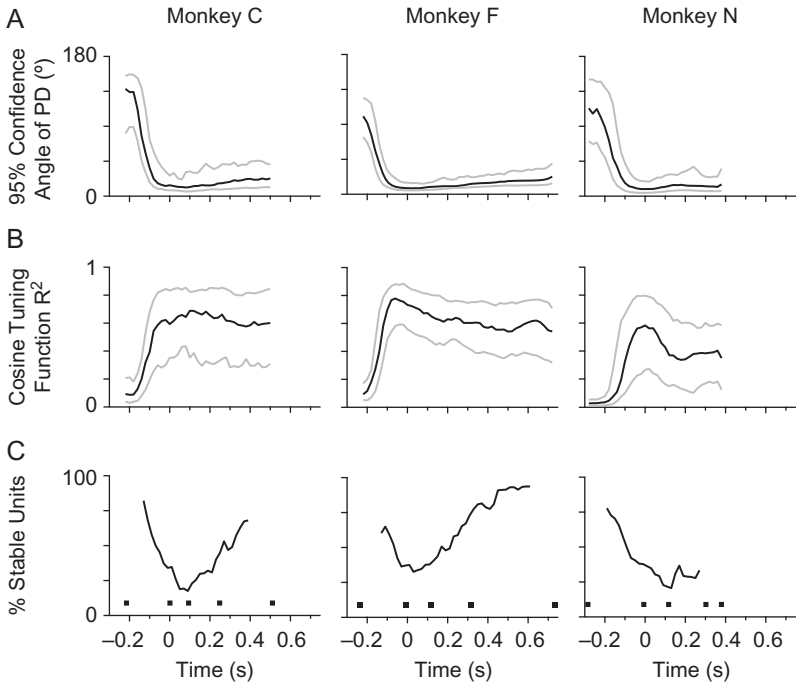

Figure 3. Stability vs. time for the population. (*A*) Reliability of PD estimates. To determine trial-to-trial variability (width of confidence interval) for each neuron and at each time bin, PDs were repeatedly estimated using a bootstrap method (see Materials and Methods). Black lines show the population median for width of PD confidence intervals (95%) computed by the bootstrap; gray lines show quartiles (Q1, Q3) for the population. The distribution began narrowing 200 ms before movement onset, with tuning becoming maximally reliable for most neurons around movement onset. (*B*) The same reliability trend was found when using R^2 for the cosine tuning regression. Tuning functions for each neuron were calculated in each 20 ms bin by averaging firing rates over task repetitions. Black and gray lines show the population median, Q1, and Q3 R^2 of the cosine fits to each neuronal tuning curve. (*C*) PD stability was assessed within 200 ms overlapping windows that were incremented in 20 ms bins. The stability test, used previously for the whole trial, was then applied to each 200 ms window for each analyzed cell. To decrease the influence of noise, bins with poor tuning ($R^2 < 0.6$) were excluded. The percentage of units with stable PDs peaked 100 ms before movement onset, decreased toward the beginning of movement, and then gradually increased toward the end of the movement when the cursor was in the target. Square markers in panel *C* correspond to target show, movement onset, peak velocity, movement offset, and reward administration.

tended to rise and fall in roughly Gaussian-shaped peaks, or components. PDs were consistent for the duration of a component, but could change abruptly from one component to the next. We, therefore, developed a model of firing rates that captured the observed Gaussian-shaped modulation and step-like cosine tuning features (Fig. 4*A*,*B*,*E*). For convenience, we chose to fit the modulation depth profile with a multi-component Gaussian function. Although this general function shape fit our data well, other forms likely could be substituted.

This model (Eq. 6) defines cosine-tuned Gaussian-shaped components, specified in part by peaks in the amplitude of the neuron's tuning function, observed at different points in time through the task. The components are further defined by a PD, which was assumed to be constant for the duration of the component (an assumption which was subsequently tested for each component). Because PDs were specified separately per component, the overall PD of the neuron was allowed to rapidly change from one component to the next. These features were simultaneously captured by the following expression, which we refer to as an epoch-specific tuning model:

$$y_i = \beta_0 + \sum_{j=1}^{J} a_j \exp\left\{\frac{-(t-\mu_j)^2}{2s_j^2}\right\}\cos(\theta_{targ} - \theta_{PD_j}) + \varepsilon_i \qquad (6)$$

Here, $y_i = \hat{\lambda}_i$ is the expected change in single-trial firing rate at each time t, given a target θ_{targ}. Baseline firing rate is denoted β_0. For each of the *J* components, the modulation depth was fitted with a Gaussian temporal profile. Thus, the *j*th width coefficient s_j specifies the standard deviation of the Gaussian profile, and the time of maximum firing rate (a_j) is given by μ_j. The term ε_i is the noise (or error) representing the deviation from the model. Once initialization parameters were obtained (see Supplemental Experimental Procedures 3), final estimates of each parameter were fit using nonlinear least squares regression for the full model given in Equation (6).

For neurons recorded from monkeys C and F, we often observed a period of tonic firing during the hold period. Monkey N was not required to hold at the target and neurons recorded during this task did not exhibit this activity. Although this activity was typically also cosine-tuned, we intentionally avoided fitting components here, as this activity was not believed to be related to the preceding movement but rather to the act of holding at the target (Kettner et al. 1988). Examples of this activity can be seen at the end of the trial period for units 59a and 79a from monkey C (Fig. 4, top row) and in Supplementary Figure 5.

PVA Analysis

The PVA was used to decode movement direction from motor cortical units. To assess the effect of tuning lability on our ability to decode movement, we reconstructed movement trajectories with 3 different formulations of the population vector.

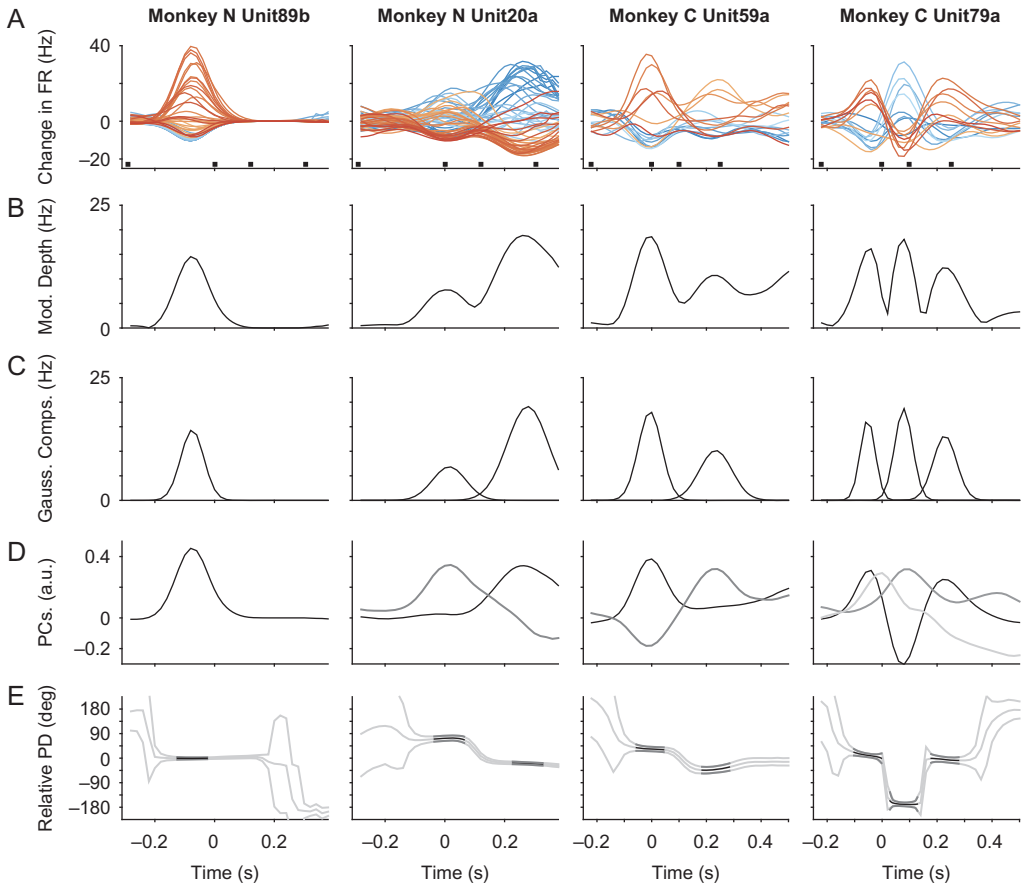

Figure 4. Episodic modulation patterns. Firing rate patterns of 4 different neuronal units are shown in columns. (*A*) The first row shows trial-averaged firing rate profiles for each target direction. Square markers correspond to alignments on target show, movement onset, peak velocity, and movement offset. (*B*) Tuning function amplitudes (estimated modulation depth, $\hat{m}_t$) calculated in each bin are shown in the second row. (*C*) Gaussian-shaped components fit to the tuning amplitudes are shown in the third row. (*D*) Eigenvectors calculated from correlation matrices across bins are shown in the fourth row (darker line intensity for eigenvectors with more explanatory power). (*E*) PDs computed repeatedly over the course of the trial are shown in the fifth row. The darkened portions highlight the 100 ms period centered on each Gaussian-shaped component and which was tested for PD stability. Error bars show the 95% CI (computed using bootstrap, see Materials and Methods).

PVA Using Initial PDs

We found that tuning becomes maximally reliable across the population of cells shortly after target onset (Fig. 3*A*,*B*). In our first formulation of the PVA, we therefore computed a single PD for each cell using the average rates in a 100 ms window of initial tuning. To account for small variations in tuning onset, and to ensure robust cosine fits, the windows were determined for each cell by finding the first 100 ms of significantly modulated activity. Population vectors were then computed for each trial using the equation:

$$P_t = \sum_i^N w_{it} C_i, \tag{7}$$

where P_t is the population vector at time t on a given trial, w_{it} is the amplitude-normalized firing rate of the ith unit at time t, and C_i is the single PD of the ith unit. To make direct comparisons between this analysis and a component-based analysis, units were included only if at least one component was successfully fitted (see Fig. 5). The time series of population vectors was integrated and averaged over task repetitions to construct a movement trajectory for each reach direction.

Component-Based PVA

Our second formulation of the PVA addressed whether PDs determined by each component in the epoch-specific tuning model would improve trajectory reconstruction. In the epoch-specific tuning model (Eq. 6), the PD of a single cell is constant during a tuning component but transitions rapidly to a new value when the component switches. We computed these component-determined PDs at each time bin for each cell using the epoch-specific tuning model fits. Population vectors were then computed using:

$$P_t = \sum_i^N w_{it} C_{it} \tag{8}$$

Here, the PD C of each unit, i, is a function of time, t.

Bin-by-bin PVA

Finally, to determine whether PD lability at a temporal resolution higher than that of the components would further improve decoding, we computed a third version of the PVA using Equation (8), but, unlike the component-based method, the PDs were computed independently in each bin.

In each of these 3 cases, we quantified the average length of the population vectors and their angular deviation from a

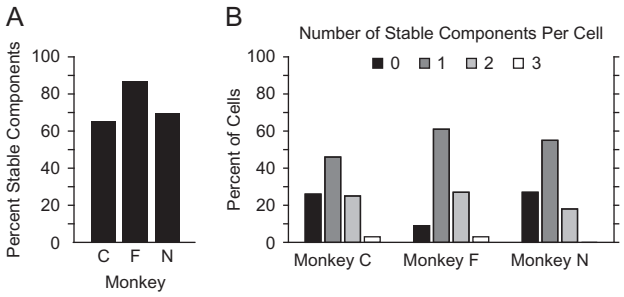

Figure 5. PD stability during component times. (*A*) Component-wise directional stability. The majority of fitted components for each monkey were found to have stable PDs for the 100 ms period centered on the component peak (see Materials and Methods for statistical method). (*B*) Number of stable components fit per neuron. The majority of components had stable PDs for at least 100 ms. When considering the number of components fit per neuron, regardless of stability, the breakdown was similar. From 0 to 3 components, the percentages for monkey C were 27, 33, 35, 4; for monkey F 6, 56, 34, 3; and for monkey N 39, 42, 18, 0. Total number of components fit for monkeys C, F, and N was 109, 161, and 146, respectively.

straight path to the target. The quality of decoding was summarized by first obtaining the length and angular deviation of the population vectors for each trial and at each time bin. All such values were then averaged. The variability in these estimates was computed via bootstrap by drawing trials randomly with replacement and re-calculating the measures using firing rates from the resampled trials. This process was repeated 1000 times.

Offline Component Recognition

In order to test the feasibility of using the component-wise PDs in a real-time population decoder, we investigated the possibility that patterns of population activity could be used to identify the tuning component driving a single unit at any given time point. This would be useful for real-time tracking of each neuron's "current" PD during online decoding experiments, based on the concurrent activity of each recorded neuron. We trained classifiers (Linear Discriminant Analysis, LDA), one separately for each unit, using the firing rates from every unit in the recorded population. That is, a feature vector at a given trial and time bin was constructed by gathering the rates of every neuron during that bin. For each unit's classifier, class labels were defined by the previously identified tuning segments, as delimited by the intersections of the adjacent components fit for that unit. The intersections were taken to be the point at which one component's amplitude became larger than the previous component's. These labels were used to train the linear discriminant classifier for that unit. Once trained, the classifier utilized the feature vector of population rates at each 20 ms sample in each trial to predict the "current" segment of the neuron's response (and thus its PD at that time). Classification was performed only for units with at least 2 components.

Additional Data Collection

Data from a fourth monkey (*M. mulatta*, male, monkey P) were collected to clarify the effect of target acquisition strategy on the observed pattern of component timing. Monkey P was trained to distinguish the stop-and-hold requirement by the color of the target, which was chosen at random for each trial. This monkey performed the task for several months prior to collecting these data. Behavioral setup, training, and array placement were comparable to those for the other 3 monkeys. Neural data were acquired and sorted using the procedures described for monkey N. Data from monkey P were pooled over 3 days of recording and included a total of 139 neurons (average 46.3 per day).

Results

Expanded Models Do Not Account for PD Lability

Data were collected as monkeys performed center-out tasks using target arrangements in 2 and 3 dimensions (Fig. 2, see also Materials and Methods). Speed profiles over each movement were bell-shaped, displacement increased monotonically and acceleration profiles were biphasic, showing that these movements are consistent with smooth point-to-point movements typical of normal reaching (Fig. 2*B*). To determine whether directional tuning changed within the task, we divided each trial into 20 ms time bins, and calculated local tuning functions for individual neurons in each bin. A PD stability test (see Materials and Methods) was used to determine whether local PDs, calculated in each bin, differed from the mean PD taken from the period 100 ms prior to movement until the end of the movement. By this criterion, only 21%, 8%, and 16% of the recorded units in monkeys C, F, and N, respectively, were found to have tuning functions that were stable throughout the task.

This temporal instability could result from a statistical interaction between direction and parameters that take on varying values throughout the task. Displacement, speed, and acceleration have characteristic temporal profiles during reaching (Fig. 2*B*). To explore the possibility that adding a combination of these kinematic terms to the regression equation could account for the observed instability of PD, we built simulations of firing rate using a mixture of kinematic variables. The resulting firing rate profiles were complex and resulted in tuning function instability through the trial (see Supplementary Fig. 2). This possibility was tested on actual data, by using the firing rates of each unit in 16 different generalized linear models consisting of different combinations of direction, position, speed, velocity, and acceleration (see Supplementary Fig. 3*A*). Although specific parameters had a slight effect on model fitness, for the most part, adding additional parameters to the basic direction-only regression had little effect on the explanatory power of the model when used on actual data, as shown by the consistent goodness-of-fit (see Supplementary Fig. 3*B*). When assessed for temporal lability in the PDs (see Supplementary Fig. 3*C*), none of the models led to a decrease in the magnitude of PD changes. Furthermore, accounting for additional kinematic terms had little effect on our statistical assessments of tuning stability for each individual neuron (see Supplementary Fig. 3*D*).

The large majority of deviations from stability in our data were small (20–40 degrees), but significant. Although our simulations showed that including a mixture of kinematic parameters could lead to directional instability, this analysis, performed on the collected data, suggests that simply expanding the basic model with more terms cannot explain the observed changes in PD.

Cosine Tuning is Robust Throughout Trials, Even in the Presence of PD Lability

We characterized tuning function stability during the task with a number of analyses. Trial-to-trial directionality in each bin was examined by selecting randomly (with replacement) firing

rates from different trials and calculating PDs repeatedly in a bootstrap procedure (Fig. 3A). Early in the trial, PD estimates for each neuron were highly unreliable (large confidence intervals), with a rapid increase in reliability about 100 ms before movement onset. A similar trend was found for the cosine tuning regression fit in each bin, where R^2 increased steeply just before movement onset (Fig. 3B). Instead of assessing directional tuning independently in separate bins, tuning stability across bins was assessed in 200 ms (10 bin) sliding windows using the PD stability test (Fig. 3C). The percentage of cells with constant PDs in the 200 ms window was relatively high (ca. 75%) early in the trial and then decreased to a minimum (ca. 25%) around movement onset, before increasing as the movement progressed. While directional tuning may not be robust early in the reach (large confidence intervals), the decrease in PD stability near movement onset occurred when the data fit the cosine tuning model well with high reliability (Fig. 3A,B). The instability of PDs by this point in the reach therefore cannot be explained by unreliable tuning or low R^2 of a cosine fit.

When testing for changes in PDs during the behavioral trials, it would appear that directional stability is related to separate portions of the task. For instance, if only the firing rates prior to movement onset are considered (−150 to −50 ms), 90%, 81%, and 74% of the units (monkeys C, F, and N) had stable PDs. However, immediately after movement onset (0–100 ms), only 35%, 72%, and 50% of units were stable.

Episodic Modulation Determines Changes in PD

As shown in Figure 1, the temporal profile of firing rate can be a determinant of directional stability. Therefore, we analyzed the modulation patterns of the recorded activity for consistent features that may be related to directional tuning. We characterized direction-related modulation by using the amplitude of the tuning function (modulation depth) calculated in each 20 ms bin throughout the task. Tuning function amplitude is shown in the second row of Figure 4 for 4 different neurons. The neuron in the first column had one clear modulation peak, the neurons in the second and third columns had an early peak followed by a later peak in modulation, and the cell in the fourth column showed 3 distinct modulation components. For each neuron, we modeled this modulation with an epoch-specific tuning model (Eq. 6) and the resulting Gaussian-shaped components are shown in the third row of Figure 4. PDs calculated within the timespan of each component were found to be stable, but these directions changed rapidly between epochs (Fig. 4, bottom row).

We next used principal components analysis (PCA) to find components of each unit's firing rate profile that covaried. This allowed us to examine prominent temporal features in the firing rate profiles without making assumptions about tuning curve shape (i.e., a cosine). Averaging across trials, we constructed a vector for each bin with components of firing rate to each target condition. We then used PCA on an T × T covariance matrix where T was the number of bins in the trial (this is sometimes referred to as "functional" PCA). The resulting eigenvectors are a function of time and represent orthogonal patterns of firing rate modulation taking place during the trials. Note that there is no consideration of directionality here, as this PCA was based solely on the variation of the observed firing rates, in contrast to the epoch-specific tuning model which was based explicitly on the typical cosine-tuning model. The 2 approaches gave very similar results: The first few eigenvectors from our PCA captured variability that was described well by the epoch-specific tuning model (Fig. 4, fourth row).

Dividing each reach into segments determined by the epoch-specific tuning fits showed that within those segments, PD was typically constant for at least 100 ms (5 time bins) as defined by our PD stability test (Fig. 5A). Within each segment, firing rates were well described by cosine tuning (see Supplementary Fig. 4A). Further, the trend toward stability was evident even when considering only the components with very good fits to a cosine function (proportion of yellow to blue in rightmost bars in Supplementary Fig. 4A). A majority of the neurons had a single stable component and units with 3 stable components were rare (Fig. 5B). When "unstable" components were analyzed, the amount of PD change was found to be quite modest despite being statistically significant (see Supplementary Fig. 4B). Possible reasons for this finding (e.g., a conservative stability criterion) and further discussion are given in Supplementary Figure 5.

The PD differences between successive components in the example neuron displayed in the fourth column of Figure 4 were approximately 180°. Although the difference in PD between components was most often statistically significant (see Supplementary Fig. 4C, blue vs. yellow), this extreme change in PD was rare. For cells with multiple components, the angles between them (see Supplementary Fig. 4C) tended to be small, with 37% having values below 45° and only 11% in the 135–180° interval.

We next considered the effect of smoothing the recorded firing rates prior to using the PD stability test. Since the test evaluates sequential time bins, smoothing the rates decreases the effective number of degrees of freedom. Given the same test statistic (Eq. 5), the frequency of type II statistical error would then increase, inflating the reported number of "stable" components. However, smoothing also reduces the amount of noise in the firing rates, which in turn changes the value of the test statistic and has the opposite effect on the outcome of the statistical test. To directly assess these opposing effects of smoothing, we again used the PD stability test on the component data, but without applying any smoothing to the firing rates (aside from binning in 20 ms bins). We found that smoothing had very little effect on the results of the stability test. For components from monkey C, we found 65% to be stable after smoothing, and 69% stable without smoothing; from monkey F, we found 87% stable after smoothing and 80% stable without smoothing; from monkey N, we found 70% stable after smoothing and 71% stable without smoothing.

To assess the sensitivity of our stability test to different amounts of PD variation in the presence of realistic noise, we generated simulated firing rates with a preset amount of PD change (see Supplementary Fig. 6A). To approximate the characteristics of our experimental data, simulated rates were matched to each recorded neuron in terms of cosine-tuning modulation depth and trial-to-trial firing rate variability. To directly compare our simulation to the experimental data, we restricted the test to 100 ms (5 bins) windows centered on each of the Gaussian-shaped components that were fit to the real data using the epoch-specific tuning model. Therefore, the simulation results are best compared with those reported in Figure 5A. Modest changes in the simulated PDs were consistently identified as "unstable" by our test (see Supplementary Fig. 6B). Given that our simulated rates were carefully matched to the real data in noise and tuning depth, this finding suggests that change in the actual PDs during these components is minimal. Indeed, if the PDs within components do change, those

changes are considerably smaller than those typically observed between components (see Supplementary Fig. 4C).

Although a cosine function described the firing rate data well at most time points, it is possible that our PD stability test was biased by imperfect fits. We therefore utilized another method for evaluating tuning stability based on the correlation between target-specific firing rates, which does not assume any parametric shape. We used this correlation metric to characterize our data in several ways, and found strong evidence for periods of stable directionality punctuated by rapid changes in tuning, without the assumption of cosine-tuning. These analyses and findings are described in detail in Supplementary Figures S7–10.

Segments of Tuning Occur at Similar Task Times Across the Population of Neurons

Next, we asked whether the timing of components was consistent across the population of recorded cells. The times in the trial of each stable component (specified by the time of the Gaussian-shaped modulation peak) were used to build histograms separately for each monkey (Fig. 6). Analysis of the histograms showed that the collective components from individual cells tended to cluster into 3 epochs within the reach trial. The timing of these global epochs was consistent across monkeys, and tuning functions calculated throughout the trial tended to have maximum amplitude and consistent PDs within these 3 epochs. Interestingly, the clustering we observed for monkeys C and F was clearly more distinct than for monkey N, and for this monkey, the probability of observing components later in the task decreased. Monkeys C and F were required to stop and hold in the target before being rewarded, while monkey N was rewarded as soon as the cursor touched the target. The behavioral significance of this event therefore differed across monkeys. Because the third directional epoch is centered around the time the target was acquired, and was less prominent in monkey N, the directionality reflected at that time may be related to arresting the movement.

To test this hypothesis, we trained a fourth monkey ("P") to perform a center-out task in which the stop-and-hold requirement was cued by target color. The monkey performed this task for several months prior to collecting behavioral and neuronal data over 3 days. We then repeated our component-fitting procedure separately for "hold" and "no hold" reach trials, fitting a total of 265 components in the "hold" task and 184 components in the "no hold" task (231 stable in the "hold" task; 143 in the "no hold" task). We found that the number of neurons with components observed in the third epoch was markedly decreased in "no hold" trials (Fig. 6, histograms for monkey P in panels A and B). Further, the separation in time of the 3 epochs was enhanced in the "hold" trials compared with "no hold" trials. This dissociation was most obvious when we combined data from the 4 monkeys and built histograms

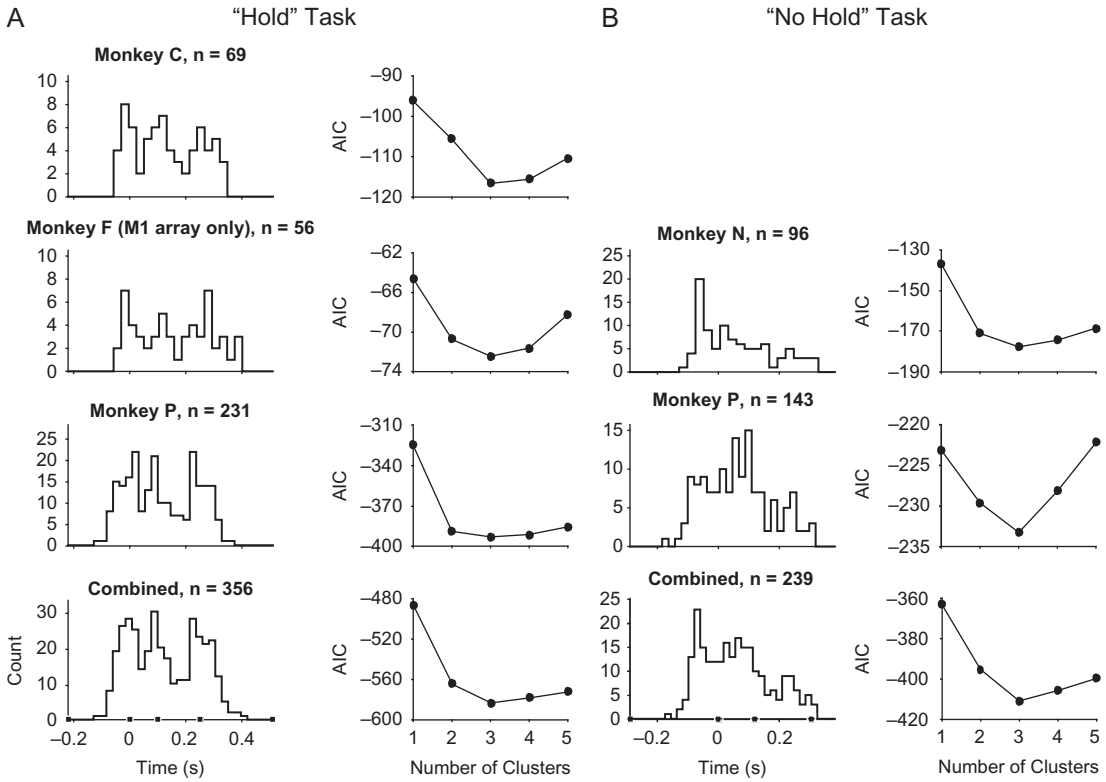

Figure 6. Temporal distribution of tuning components. The timings of Gaussian-shaped peaks from "stable" components were used to make histograms of component occurrence for each monkey (left columns in *A* and *B*). Gaussian mixture models were fit to component times, and the Akaike information criterion (AIC) was computed for fits with 1 through 5 clusters (right columns in *A* and *B*). We consistently observed a minimum AIC for 3 clusters, suggesting components fall into 1 of 3 epochs, which are similar across monkeys. (*A*) Stable component times observed during "hold" tasks. (*B*) Stable component times observed during "no hold" tasks. Histograms in the bottom row of *A* and *B* represent data pooled from each preceding histogram. The 3 epochs are most distinctive in the "hold" task, but can also be observed in the "no hold" task. Movement begins at Time = 0 and the filled square symbols denote the behavioral events of target show, peak velocity, movement offset, and end of hold (if relevant). The time scales in *A* have been scaled linearly between event times to match those of monkey C; time scales in *B* have been scaled to match monkey N.

separately for the 2 task requirements (Fig. 6A,B, bottom row). Requiring an accurate target acquisition prolonged the last phase of the reach, as we found that monkey P entered the target zone 43 ms sooner in the "no hold" trials than in the "hold" trials, measured relative to movement onset (*t*-test, $P = 3.3 \times 10^{-79}$, $t = 19.4$, df = 3391, 95% CI = [38 ms, 47 ms]). These results support the idea that the third component is associated with the terminal portion of the reach.

Regardless of task type, the earliest period of stable tuning began about 100 ms before movement onset, and peaked about 50 ms later. The timing of the second epoch peaked later in the reach, about 50 ms before the arm reached its peak velocity. The third epoch began around peak velocity and peaked approximately at the end of the movement. Most cells had a single modulation peak that contributed to one of the 3 epochs, although some cells had multiple directional components that fit into these epochs. Those cells with directional firing in an epoch tended to have stable PDs within that period. As shown by our tuning function analyses (Fig. 3A,B), directional tuning is not evident early in the trial. The sharp increase in tuning function fit about 100 ms before movement onset corresponds to the beginning of the first global tuning component which peaks about 50 ms before movement onset (Fig. 6). A second, separate directional feature peaks subsequently, overlapping the first, so that 2 strong and sequential directional signals in the neural population are evident during the reach. Single neurons driven by both signals could be found to have temporally distinct tuning functions with different PDs (for example, the units in the middle 2 columns of Fig. 4).

Accounting for Tuning Changes can be Important for Accurately Decoding Reach Trajectory

The concept of directional tuning in the motor cortex has received a great deal of support since its introduction in the early 1980s (for a review- Georgopoulos and Carpenter 2015). One of the first population vector demonstrations showed that the representation of direction evolved and pointed consistently to the target during center-out reaches (Georgopoulos et al. 1984). Following that work, neural trajectories were constructed by adding the time-series of population vectors tip-to-tail, and were found to closely match the trajectory of the arm when reaching to targets (Georgopoulos et al. 1988) and when drawing a variety of figures (Schwartz 1993, 1994a, 1994b; Moran and Schwartz 1999; Schwartz and Moran 1999).

How could such a large body of work, based on the idea of a fixed PD, produce successful movement predictions if the tuning function is labile? Because the typical tuning model is a cosine, the firing rate average over multiple epochs of cosine tuning is also well-described by a cosine, even if PD changes occur between epochs (see Supplementary Fig. 11). As is the case with many center-out reports, using this average PD in the PVA yields accurate decoding, tending to minimize the errors due to PD changes between epochs. We found that directional tuning begins 100 ms before movement onset and extends beyond the end of movement. Using the amplitude of directional tuning, we identified 3 separate epochs. Within each epoch, PD was constant. The first 2 epochs spanned the initial portion of the reach. A change in PD within this span is rare; most cells had only one modulation component (occurring in the first or second global epoch) in this peri-movement period. Indeed, when we restricted our data sample to this portion of the task, trajectories decoded with population vector analysis were accurate (see Supplementary Table 1B). Because confining the data to this portion of the task is common practice, the issue of labile PD has not been identified as a major problem in decoding experiments. Most of the directional lability found in our data samples came from the early reaction time portion of the task when directional drive was weak, or later in the task as the target was acquired and held, which may be a phase distinct from the initial portion of the movement. It should be noted that our analyses focused on directional modulation and this may differ substantially from overall firing rate modulation. Casual examination of our data suggests that firing rate modulation tends to decrease through the reach, while directional modulation (e.g., in the third component) may still be significant. Since the PVA is based on firing rate modulation, distortions of the neural trajectory toward the end of the reach due to changes in PD may be marginalized by lower firing rates.

As a linear decoder, the population vector is optimal when neurons have cosine tuning functions and the recorded sample has a uniform distribution of PDs (Salinas and Abbott 1994; Kass et al. 2005). Deviations from cosine-tuning will lead to inaccuracies in the decoded movement. Furthermore, when the PD of a neuron changes during a movement, trajectories decoded from a time-series of population vectors can be distorted if these non-stationarities are not taken into account. Population vector trajectories were constructed for the reaches performed by each monkey (see Materials and Methods). Results from monkey C are shown in Figure 7. When neural trajectories were constructed with a single PD taken as the initial occurrence of significant tuning, the neural trajectories were distorted and shortened in the 10 and 4 o'clock directions (Fig. 7A). However, use of component-wise PDs in the corresponding portion of each trial led to more accurate population vectors (Fig. 7B, see Supplementary Table 1A). It could be argued that if a cell's directionality changed constantly during a reach, the most accurate reconstruction could be achieved using PDs with a high temporal resolution. To test this idea, we calculated PDs in each bin for every cell in the sample, and computed the trajectories in Figure 7C. These reconstructed trajectories were only slightly better than those generated with the component-wise PDs (Fig. 7B), suggesting that the components adequately captured the changes in directionality that lead to decoding errors. It should be noted, however, that these considerations apply mostly to the last portion of the trajectory. If the analysis is confined to the portion of each trial defined by the first 2 global components (Fig. 6) around the

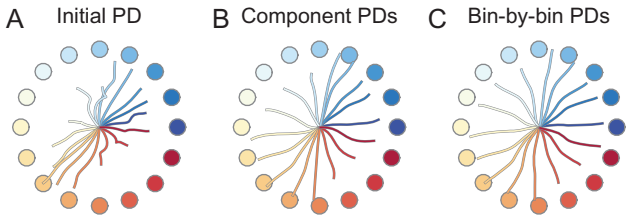

Figure 7. Population vector reconstructions of cursor trajectories to 16 center-out targets for monkey C. Neural trajectories were generated by calculating population vectors in each bin (from 100 ms prior to movement until 100 ms prior to end of trial) and adding the vectors tip-to-tail. Target colors are as in Figure 2. (A) The population vectors were calculated using a single, initial PD for each neuron. This method resulted in highly distorted trajectories. (B) PDs from within each component (see Materials and Methods) were used to construct the population vectors. This method largely remedied the distortions seen in A. (C) Tuning functions were calculated in each time bin and their PDs were used for the neural trajectories. This method yielded only modest improvements over the method used in B.

time of movement, using a single PD for that epoch was almost as effective as using separate components (see Supplementary Table 1B).

Offline Identification of System State Enhances Accurate Decoding

Assuming that the directional components effect changes in directionality simultaneously for many neurons, it should be possible to identify, at any point in time, which component is acting as the current driver on a neuron. The identity of the component could then be used as an index to the unit's component-wise PD. Using each cell's segment-specified PD would be expected to generate a more accurate readout of the arm's direction than a prediction produced with a single PD. This real-time readout would be useful, for instance, in neural prosthetics. To demonstrate the utility of this approach, the "current" tuning segment of each neuron was detected on each trial and in each time bin by using the concurrent activity of all simultaneously recorded units in a linear-discriminant analysis. This showed that the individual components of neurons could be identified with high accuracy for the 3 monkeys (Fig. 8).

To illustrate the feasibility of real-time decoding of movement trajectory using the components model, we performed an additional PVA analysis (based on Equation 8 in Materials and Methods). In this version, the PD at every time step in each individual trial was defined by the PD of the component detected by the LDA for that sample. The identified components, when used to specify each neuron's PD (per trial and time bin), produced population vectors that were comparable to those in Fig. 7B. We used a bootstrap procedure to compare the magnitude and angular accuracy of population vectors computed this way with those computed using the true labels. The results of this method did not significantly differ from those using each cell's "ground truth" components (bootstrap test, $P > 0.05$ for each monkey).

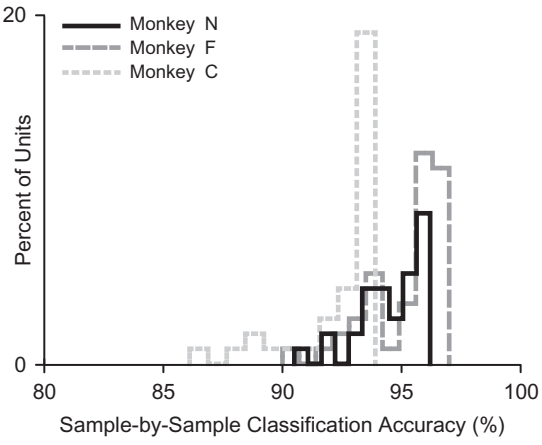

Figure 8. Offline component recognition. We investigated the possibility that patterns of population activity could be used to identify the tuning segment (component) of each single unit at any given moment in a trial. We trained classifiers (LDA), one for each unit, using the concurrent firing rate samples from every simultaneously recorded unit. For each unit's classifier, samples in each bin were labeled based on their timing, relative to the unit's previously fitted components, with transitions delimited by the point at which one component's amplitude became larger than the previous component's. These labels were used to train the linear discriminant classifier for that unit, which was then used to predict the "current" temporal epoch for each 20 ms sample during each trial. Five-fold cross-validated success rates for units with at least 2 components were high: 94.7 ± 1.4%, 95.2 ± 1.6%, and 92.5 ± 2.0% for monkeys N, F, and C, respectively. Histograms of success rate per unit are displayed for each monkey. Success rate by chance was computed by randomly shuffling the group labels prior to training the classifiers, and yielded much worse classification: 50.1% ± 0.3, 48.8 ± 5.1%, and 48.2 ± 5.4% for monkeys N, F, and C, respectively.

Discussion

Although the center-out task invariably shows that the mean discharge rate of neurons is tuned to movement direction, variations of the task in which consideration of speed/amplitude (Churchland and Shenoy 2007), shifts in workspace location (Caminiti et al. 1990), movement fragments (Hatsopoulos et al. 2007), isometric hand forces (Sergio and Kalaska 1998, 2003), arm posture (Scott and Kalaska 1995), limb biomechanics (Suminski et al. 2015), and covert encoding perturbations during brain-controlled tasks (Jarosiewicz et al. 2008) have shown that directional tuning functions are labile. Since some of this directional instability has been found within single reaches, concerns have been raised that the apparent representation of movement direction may be secondary to other aspects of motor control such as force generation (Sergio et al. 2005), oscillatory dynamics (Shenoy et al. 2013), or intrinsic skeletal-muscular action (Suminski et al. 2015). One of these papers (Suminski et al. 2015), using a center-out task, reported rapid changes in motor cortical PDs around movement onset, a finding that is congruent with the transition between components 1 and 2 found in our work. Instead of attributing this transition to behavioral aspects of the task, these investigators suggested that the PD changes were related to successive recruitment of different muscles during the task, with the argument that the primary determinant of a motor cortical neuron's PD is the set of muscles to which it is connected. The primacy of motor cortical activity as a driver of muscle contraction has been controversial since the original characterization of this cortical structure (Fritsch and Hitzig 1870). While motor cortical output undoubtedly has a role in altering muscle excitability, it is equally clear that there is no simple correspondence between a neuron's firing rate and the excitability of its "muscle field" (i.e., "upper motoneurons") (Phillips and Porter 1997), even for the small portion of the corticofugal output that projects monosynaptically to spinal motoneurons (Griffin et al. 2015). The historic issue of whether the motor cortex operates as a direct link to muscles or has a large role in movement planning is rooted in the assumption that a single function needs to be assigned to this anatomical structure.

Current theories of motor control link displacement, the generation of muscle activity, and behavioral output into a cohesive scheme (for a review see Diedrichsen et al. 2010). In this approach, the intended state of the arm (e.g., position and velocity) is transformed by an "internal model" to a set of muscle activations, which, in turn, displace the limb as an action on the external world. Sensation from the movement is then fed back to the system. The modeled transformations are serial with the expectation that they correspond to the purported hierarchical anatomical connectivity between brain structures. Advocates of direct cortical participation in muscle contraction equate the motor cortex with the internal model, as the place where kinematics are transformed to muscle activation. Despite the attraction of these control schemes, neurophysiological results do not support the correspondence between separate brain structures and the discrete operational components used to construct these models. Multiple brain structures at different levels of the proposed hierarchy have similar directional

characteristics (Kalaska et al. 1983; Kutz et al. 1997; Turner and Anderson 1997; Johnson et al. 2001; Suminski et al. 2015). Describing specific aspects of function is useful for framing concrete motor control issues, but localizing function to specific portions of the neural substrate may have less utility. The assignment of a single specific role to the motor cortex may be incompatible with the functional dynamics of the motor system.

There has been renewed interest in treating point-to-point reaches in the context of a dynamical system. The original idea was that an equilibrium position, defined by the joint angle where the forces of opposing muscles balance, could be preset before the movement began (Feldman 1966; Polit and Bizzi 1978). When the arm was released, achieving this equilibrium would require no further input. A definitive experiment (Bizzi et al. 1984) disproved this idea, although modifications based on the idea of stable equilibria (Hogan 1984; Flash 1987) have since gained traction. More recently the "set and forget" control concept of reaching has been revived (Churchland et al. 2012). This recent rendition posits that trajectory specification takes place during the pre-movement period, and upon movement initiation the inherent properties of the system move the arm to a target. This concept can be described by a dynamical system formalism:

$$\dot{\lambda} = C\lambda + Du;$$

where λ is firing rate (the system's state variable) and u is the trajectory specification (the system's input). The term C transforms the current firing rate to a "change" in firing rate; $C\lambda$ describes the component of firing rate change that depends on the current firing rate itself. Similarly, D transforms the intended trajectory u to a change in firing rate. The integral of the first term, $\int C\lambda\, dt$, is referred to as the "natural response" and that of the second term, $\int Du\ dt$, as the "forced response." In the recent "set and forget" concept, $u = 0$ during the movement; desired velocity acts as an input before the movement begins with subsequent movement executed by the "engine of movement" in the absence of input. Indeed, we see non-step like modulation of firing rate during the reaching task (e.g., Fig. 1A). Since this is not accounted for by different combinations of movement parameters, our results suggest that there is a system-dependent structure to motor cortical activity. While this suggests that a putatively constant direction signal can elicit a time-varying change in firing rate, our results also show that encoding of directional input is consistently maintained during discrete epochs of stable directional tuning throughout the movement. While this study cannot rule out the possibility that these directional signals are components of the natural response, our results are consistent with control linked to behavioral drivers associated with separate states occurring during the task.

Neural operations are likely to be determined by the different control criteria needed during behavior. For instance, reaching is characterized by a set of invariants or "neural constraints" (Bernstein 1984). A behavioral perspective can help link our findings of directional states in neural populations to global control issues. For goal-directed reaching, an initial phase, characterized by a stereotypical bell-shaped velocity profile (Morasso 1981), during which the hand moves almost to the target, is too rapid for visual feedback to act concurrently (Hollerbach 1982). Subsequently, a distinct terminal phase takes place, during which the hand and target are foveated together (Soechting and Lacquaniti 1981; Meyer et al. 1988; Milner 1992). Different cortical mechanisms may operate in these phases (Brinkman and Kuypers 1972; Paillard 1982). The first directional epoch we identified corresponds to the reaction time, the second peaks in the initial transport phase, and the last component is linked to target acquisition. Recent studies based on correlational structure between units within a recorded population suggest that this structure changes at the onset of an arm movement (Kaufman et al. 2014; Sussillo et al. 2015). Another experiment using a reach-to-grasp task has shown that there is a clear transition in motor cortical activity correlation from object location to object type at the end of the reach (Rouse and Schieber 2016). Analysis of firing rates using Hidden Markov Models during a reaching task supports the idea of stable regimes and sharp state transitions taking place in the control system (Abeles et al. 1995). Together, these findings support the concept of discrete processes taking place sequentially through a task. By recognizing consistent non-stationarities in the time-varying patterns of neural activity associated with motor control, we can better describe details of the processing used to generate behavior.

Supplementary Material

Supplementary data is available at *Cerebral Cortex* online.

Funding

The National Institutes of Health (R01-NS047356, R01-NS050256, RC1-NS070311); and Defense Advanced Research Projects Agency (W911NF-06-1-0053, N66001-10-C-4056, N66001-12-C-4027).

Authors' Contributions

S.B.S. and J.O. made equal contributions in analyzing the data and writing drafts of the paper. A.J.C.M. collected data, performed initial data analyses, and wrote initial drafts of the manuscript. G.W.F. collected data and contributed to the analyses. Z.L. contributed to the analyses. M.V., S.M.C., and R.E.K. gave analytical advice. A.B.S. conceived the study, participated in the data analysis, and drafted the paper.

Notes

The authors wish to thank Valerie Ventura for her analytical advice, Jeong-Woo Sohn, Andrew Whitford, and Robert Rasmussen for collecting data used in this paper, and Scott Kennedy for helpful discussions. The authors declare no competing financial interests. *Conflict of Interest*: None declared.

References

Abeles M, Bergman H, Gat I, Meilijson I, Seidemann E, Tishby N, Vaadia E. 1995. Cortical activity flips among quasi-stationary states. Proc Natl Acad Sci USA. 92:8616–8620.

Ashe J, Georgopoulos AP. 1994. Movement parameters and neural activity in motor cortex and area 5. Cereb Cortex. 6: 590–600.

Bernstein NA. 1984. The problem of the interrelation of coordination and localization. In: Whiting HTA, editor. Human motor actions. Bernstein reassessed (Advances in Psychology 17). Amsterdam (North Holland): Elsevier. p. 77–119.

Bizzi E, Accornero N, Chapple W, Hogan N. 1984. Posture control and trajectory formation during arm movement. J Neurosci. 4(11):2738–2744.

Brinkman J, Kuypers HG. 1972. Splitbrain monkeys: cerebral control of ipsilateral and contralateral arm, hand, and finger movements. Science. 176:536–539.

Caminiti R, Johnson PB, Urbano A. 1990. Making arm movements within different parts of space: dynamic aspects in the primate motor cortex. J Neurosci. 10(7):2039–2058.

Churchland MM, Cunningham JP, Kaufman MT, Foste JD, Nuyujukian P, Ryu SI, Shenoy KV. 2012. Neural population dynamics during reaching. Nature. 487:51–56.

Churchland MM, Shenoy KV. 2007. Temporal complexity and heterogeneity of single-neuron activity in premotor and motor cortex. J Neurophysiol. 97:4235–4257.

Diedrichsen J, Shadmehr R, Ivry RB. 2010. The coordination of movement: optimal feedback control and beyond. Trends Cogn Sci. 14:31–39.

Feldman A. 1966. Functional tuning of the nervous system with control of movement or maintenance of a steady posture. II. Controllable parameters of the muscle. Biophysics (Oxf). 11: 565–578.

Flash T. 1987. The control of hand equilibrium trajectories in multi-joint arm movements. Biol Cybern. 57:257–274.

Fraser GW, Schwartz AB. 2012. Recording from the same neurons chronically in motor cortex. J Neurophysiol. 107: 1970–1978.

Fritsch G, Hitzig E. 1870. Electric excitability of the cerebrum. Arch Anat Physiol Wissen. 37:300–332.

Georgopoulos AP, Caminiti R, Kalaska JF, Massey JT. 1983. Spatial coding of movement: a hypothesis concerning the coding of movement direction by motor cortical populations. Exp Brain Res Suppl. 7:327–336.

Georgopoulos AP, Carpenter AF. 2015. Coding of movements in the motor cortex. Curr Opin Neurobiol. 33:34–39.

Georgopoulos AP, Kalaska JF, Caminiti R, Massey JT. 1982. On the relations between the direction of two-dimensional arm movements and cell discharge in primate motor cortex. J Neurosci. 2(11):1527–1537.

Georgopoulos AP, Kalaska JF, Crutcher MD, Caminiti R, Massey JT. 1984. The representation of movement direction in the motor cortex: single cell and population studies. In: Edelman GM, Goll WE, Cowan WM, editors. Dynamic aspects of neocortical function. New York (NY): Neurosciences Research Foundation, Inc. p. 501–524.

Georgopoulos AP, Kettner RE, Schwartz AB. 1988. Primate motor cortex and free arm movements to visual targets in three-dimensional space. II. coding of the direction of movement by a neuronal population. J Neurosci. 8:2928–2937.

Griffin DM, Hoffman DS, Strick PL. 2015. Corticomotoneuronal cells are “functionally tuned”. Science. 350:667–670.

Hatsopoulos NG, Xu Q, Amit Y. 2007. Encoding of movement fragments in the motor cortex. J Neurosci. 27: 5105–5114.

Hochberg LR, Serruya MD, Friehs GM, Mukand JA, Saleh M, Caplan AH, Branner A, Chen D, Penn RD, Donoghue JP. 2006. Neuronal ensemble control of prosthetic devices by a human with tetraplegia. Nature. 442:164–171.

Hogan N. 1984. Adaptive control of mechanical impedance by coactivation of antagonist muscles. IEEE Trans Autom Control. 29:681–690.

Hollerbach JMM. 1982. Computers, brains and the control of movement. Trends Neurosci. 5:189–192.

Jarosiewicz B, Chase SM, Fraser GW, Velliste M, Kass RE, Schwartz AB. 2008. Functional network reorganization during learning in a brain-computer interface paradigm. Proc Natl Acad Sci USA. 105:19486–19491.

Johnson MT, Mason CR, Ebner TJ. 2001. Central processes for the multiparametric control of arm movements in primates. Curr Opin Neurobiol. 11:684–688.

Kalaska JF, Caminiti R, Georgopoulos AP. 1983. Cortical mechanisms related to the direction of two-dimensional arm movements: relations in parietal area 5 and comparison with motor cortex. Exp Brain Res. 51:247–260.

Kass RE, Ventura V, Brown EN. 2005. Statistical issues in the analysis of neuronal data. J Neurophysiol. 94:8–25.

Kaufman MT, Churchland MM, Ryu SI, Shenoy KV. 2014. Cortical activity in the null space: permitting preparation without movement. Nat Neurosci. 17:440–448.

Kettner RE, Schwartz AB, Georgopoulos AP. 1988. Primate motor cortex and free arm movements to visual targets in three-dimensional space. III. positional gradients and population coding of movement direction from various movement origins. J Neurosci. 8(8):2938–2947.

Kutz DF, Dannenberg W, Werner W, Hoffmann KP. 1997. Population coding of arm-movement-related neurons in and below the superior colliculus of Macaca mulatta. Biol Cybern. 76:331–337.

Meyer DE, Abrams RA, Kornblum S, Wright CE, Smith JEK. 1988. Optimality in human motor performance: ideal control of rapid aimed movements. Psychol Rev. 95:340–370.

Milner TE. 1992. A model for the generation of movements requiring endpoint precision. Neuroscience. 49:487–496.

Moran DW, Schwartz AB. 1999. Motor cortical activity during drawing movements: population representation during spiral tracing. J Neurophysiol. 82:2693–2704.

Morasso P. 1981. Spatial control of arm movements. Exp Brain Res. 42:223–227.

Paillard J. 1982. The contribution of peripheral and central vision to visually guided reaching. In: Ingle DJ, Goodale MA, Mansfield RJW, editors. Analysis of visual behavior. Cambridge: MIT Press. p. 367–385.

Phillips CG, Porter R. 1997. Corticospinal neurons. London: Academic Press.

Polit A, Bizzi E. 1978. Processes controlling arm movements in monkeys. Science. 29:1235–1237.

Rouse AG, Schieber MH. 2016. Spatiotemporal distribution of location and object effects in primary motor cortex neurons during reach-to-grasp. J Neurosci. 36(41):10640–10653.

Salinas E, Abbott LF. 1994. Vector reconstruction from firing rates. J Comput Neurosci. 1:89–107.

Schwartz AB. 1993. Motor cortical activity during drawing movements: population response during sinusoid tracing. J Neurophysiol. 70:28–36.

Schwartz AB. 1994a. Direct cortical representation of drawing. Science. 265:540–542.

Schwartz AB. 1994b. Neuronal substrate for volitional movement. In: Bennett KMB, Castiello U, editors. Insights into the reach to grasp movement. Amsterdam (North Holland): Elsevier. p. 59–83.

Schwartz AB, Moran DW. 1999. Motor cortical activity during drawing movements: population representation during lemniscate tracing. J Neurophysiol. 82:2705–2718.

Scott SH, Kalaska JF. 1995. Changes in motor cortex activity during reaching movements with similar hand paths but different postures. J Neurophysiol. 73:2563–2567.

Sergio LE, Hamel-Pâquet C, Kalaska JF. 2005. Motor cortex neural correlates of output kinematics and kinetics during isometric-force and arm-reaching tasks. J Neurophysiol. 94: 2353–2378.

Sergio LE, Kalaska JF. 1998. Changes in the temporal pattern of primary motor cortex activity in a directional isometric

force versus limb movement task. J Neurophysiol. 80: 1577–1583.
Sergio LE, Kalaska JF. 2003. Systematic changes in motor cortex cell activity with arm posture during directional isometric force generation. J Neurophysiol. 89:212–228.
Serruya MD, Hatsopoulos NG, Paninski L, Fellows MR, Donoghue JP. 2002. Instant neural control of a movement signal. Nature. 416:141–142.
Shenoy KV, Sahani M, Churchland MM. 2013. Cortical control of arm movements: a dynamical systems perspective. Annu Rev Neurosci. 36:337–359.
Soechting JF, Lacquaniti F. 1981. Invariant characteristics of a pointing movement in man. J Neurosci. 1:710–720.
Suminski AJ, Mardoum P, Lillicrap TP, Hatsopoulos NG. 2015. Temporal evolution of both premotor and motor cortical tuning properties reflect changes in limb biomechanics. J Neurophysiol. 113:2812–2823.
Sussillo D, Churchland MM, Kaufman MT, Shenoy KV. 2015. A neural network that finds a naturalistic solution for the production of muscle activity. Nat Neurosci. 18: 1025–1033.
Taylor DM, Helms Tillery SI, Schwartz AB. 2002. Direct cortical control of 3D neuroprosthetic devices. Science. 296: 1829–1832.
Turner RS, Anderson ME. 1997. Pallidal discharge related to the kinematics of reaching movements in two dimensions. J Neurophysiol. 77:1051–1074.
van Hemmen JL, Schwartz AB. 2008. Population vector code: a geometric universal as actuator. Biol Cybern. 98:509–518.
Wessberg J, Stambaugh CR, Kralik JD, Beck PD, Laubach M, Chapin JK, Kim J, Biggs SJ, Srinivasan MA, Nicolelis MA. 2000. Real-time prediction of hand trajectory by ensembles of cortical neurons in primates. Nature. 408:361–365.
Wodlinger B, Downey JE, Tyler-Kabara EC, Schwartz AB, Boninger ML, Collinger JL. 2015. Ten-dimensional anthropomorphic arm control in a human brain-machine interface: difficulties, solutions, and limitations. J Neural Eng. 12:1–17.